Beyond the pair approximation: Modeling colonization population dynamics

Ignacio A. Rodriguez-Brenes,[1,*] Dominik Wodarz,[2] and Natalia L. Komarova[1,†]
[1]*Department of Mathematics, University of California Irvine, Irvine, California 92697, USA*
[2]*Department of Population Health and Disease Prevention, University of California, Irvine, California 92617, USA*

(Received 17 June 2019; revised manuscript received 27 September 2019; accepted 2 January 2020; published 6 March 2020)

The process of range expansion (colonization) is one of the basic types of biological dynamics, whereby a species grows and spreads outwards, occupying new territories. Spatial modeling of this process is naturally implemented as a stochastic cellular automaton, with individuals occupying nodes on a rectangular grid, births and deaths occurring probabilistically, and individuals only reproducing onto unoccupied neighboring spots. In this paper we derive several approximations that allow prediction of the expected range expansion dynamics, based on the reproduction and death rates. We derive several approximations, where the cellular automaton is described by a system of ordinary differential equations that preserves correlations among neighboring spots (up to a distance). This methodology allows us to develop accurate approximations of the population size and the expected spatial shape, at a fraction of the computational time required to simulate the original stochastic system. In addition, we provide simple formulas for the steady-state population densities for von Neumann and Moore neighborhoods. Finally, we derive concise approximations for the speed of range expansion in terms of the reproduction and death rates, for both types of neighborhoods. The methodology is generalizable to more complex scenarios, such as different interaction ranges and multiple-species systems.

DOI: 10.1103/PhysRevE.101.032404

I. INTRODUCTION

Range expansion, or colonization, is the process in biology by which a species spreads to new areas. Examples include the growth of microorganisms to form two-dimensional (2D) formations called biofilms [1]; the spread of solid tumors in two and three dimensions [2] (including the formation of spheroids in vitro [3] and the growth of cell cultures in two and three dimensions [4]); the growth of bacterial and viral/bacteriophage plaques [5–7]; and even the growth of human settlements [8,9]. It is well known that spatial population expansion is very different from the exponential growth experienced by well mixed systems, and yet mathematical tools appropriate for the description of range expansion are not fully developed.

Mathematical models of colonization processes vary in methodology and sophistication. One popular approach is to use stochastic cellular automata. See [10], for example, for a review of their use in tumor modeling, [11] for a review of applications to urban development, and also [2,12–14]. In these models, individuals are located on a fixed grid, and stochastic rules govern births and deaths. This versatile approach has proven to be a valuable tool for computational studies of range expansion and various related phenomena. It is conceptually simple, but also a significant improvement compared to ordinary differential equations (ODEs), because it is both stochastic and spatial. This approach, however, can be computationally very costly, making it difficult to extract from simulations statistics on the time-evolution of a system, especially when population sizes are large. Furthermore, exact analytical descriptions of these models, such as those obtain via the Kolmogorov or master equations [15] are usually intractable.

Some of the most common simplified descriptions of cellular automata (also known as agent-based models) are derived from mean-field behavior. These include deterministic reaction-diffusion equations, such as Fisher's equation [16]. Mean-field approximations, however, neglect the important effects of spatial correlations. As a consequence most of these models provide inaccurate descriptions of the average trajectories of stochastic agent-based models. The next level of complexity is the so called pair approximation; see, e.g., [17–24]. This methodology has been used in an attempt to capture certain aspects of spatial dynamics by more tractable means. It can be successful at predicting equilibrium properties of a system, but in general does not provide good time-series agreement with the corresponding stochastic process [25].

In this paper we develop deterministic spatially explicit approximations for the expected trajectories of a two-dimensional stochastic birth-death process implemented as an agent-based model. The approximations provide an accurate description of the expected time evolution of the system. In particular, we focus on modeling population growth expanding radially from an origin o, and compare our results with the traditional pair approximation and mean-field models.

We also derive simple approximate formulas for the steady-state population densities based on the death rate, D, and reproduction rate, L, of individuals. While in a well-mixed nonspatial setting (mass action), the equilibrium density, ρ_{ma}, is given by

$$\rho_{ma} = 1 - \frac{D}{L}, \tag{1}$$

*Corresponding author: ignacio.rodriguezbrenes@uci.edu
†Corresponding author: komarova@uci.edu

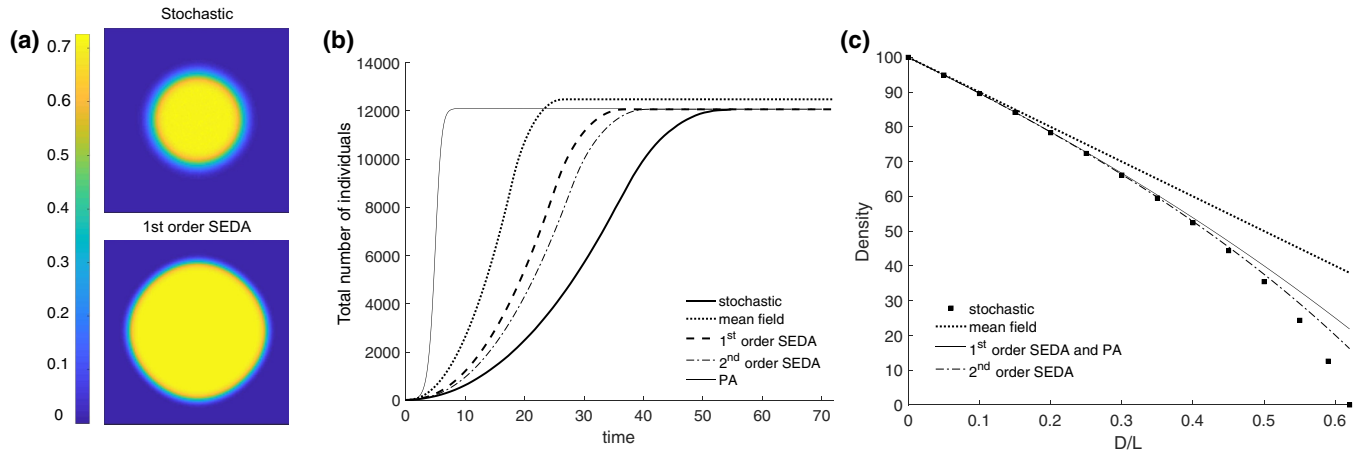

FIG. 1. (a) Spatial configuration of the expected population density at $t = 19.5$, for the stochastic (top) and first-order SEDA (bottom) models. The color bar indicates density. (b) Expected total number of individuals as a function of time. Results from stochastic simulations (thick solid line) compared with the output of the mean-field model, first- and second-order SEDA, and pair approximation (PA, thin solid line). In panels (a) and (b), death rate $D = 1$; reproduction rate $L = 4$; grid size 129×129. Initial conditions: 5 individuals at grid's center. (c) Steady-state density of occupied sites as a function of the death-to-birth ratio D/L. Stochastic results based on 10^4 or more independent simulations per point/curve. Initial conditions: 13 individuals at grid's center. Confidence interval error bars are smaller than thickness of symbols/curves (not shown).

in spatially restricted populations this quantity is lower. We find that in the case of the von Neumann neighborhood (four neighbors), the density can be approximated by

$$\rho_{vN} = \left(3 - 4\frac{D}{L}\right)\left(3 - \frac{D}{L}\right)^{-1} \tag{2}$$

(where the subscript vN stands for "von Neumann"), in the case of the hexagonal (honeycomb) lattice, where each node has six nearest neighbors, we have

$$\rho_{H} = \left(5 - 6\frac{D}{L}\right)\left(5 - \frac{D}{L}\right)^{-1} \tag{3}$$

(where H stands for "hexagonal"), and in the case of the Moore neighborhood (eight neighbors), it is approximately given by

$$\rho_{M} = \left(7 - 8\frac{D}{L}\right)\left(7 - \frac{D}{L}\right)^{-1} \tag{4}$$

(where the subscript M stands for "Moore"). The general formula that describes these spatial approximations is

$$\rho(n) = \left(n - 1 - n\frac{D}{L}\right)\left(n - 1 - \frac{D}{L}\right)^{-1}, \tag{5}$$

where n is the number of neighbors in the grid's geometry. This formula holds also for a 3D square lattice, for both the Moore and von Neumann neighborhoods. Note that in (5) the limit as $n \to \infty$ recovers the equilibrium density for mass action (1), where the number of neighbors is infinite.

Finally, we develop concise approximations for the expected speed of range expansion in an infinite grid. We end by discussing extensions of the theory—including three-dimensional growth, different grid geometries, and multiple species—and several important evolutionary and biological applications.

II. SPATIALLY EXPLICIT DECOUPLING APPROXIMATIONS

A. Preliminaries

We begin by considering a birth-death process on a 2D rectangular lattice. Let the value of the site with coordinates (i, j) at time t be $x_{ij}(t) = 0$ if the site is empty and $x_{ij}(t) = 1$ if it is occupied. We consider the ℓ_1 distance in the lattice, i.e., $\mathrm{dist}(x_{ij}, x_{lk}) = |i - l| + |j - k|$. Defining nearest neighbors as sites that lie one unit of distance apart from each other, we introduce a notation for the four nearest neighbors of a site x_{ij}: We write $x_{ij}^{(1)} = x_{i-1,j}$, $x_{ij}^{(2)} = x_{i+1,j}$, $x_{ij}^{(3)} = x_{i,j-1}$, $x_{ij}^{(4)} = x_{i,j+1}$. Note that a site and its four nearest neighbors make up a von Neumann neighborhood of radius 1. Finally, we assume that individuals reproduce stochastically onto each unoccupied nearest neighboring site with a rate $L/4$, and die at a rate D.

Figure 1(b) plots the expected number of individuals as function of time. We implement the process as a stochastic agent-based model on a finite grid with periodic boundary conditions using the next reaction method [26] (thick solid line). Here, starting from an initial small cluster of cells at the grid's center, the expected number of individuals first increases and then plateaus as the population colonizes the entire grid. Figure 1(a) depicts, as a heatmap, the spatial configuration of the expected number of individuals at a time before the entire grid is colonized.

If we use angular brackets to denote the expected value, we find that the stochastic process results in the following equation:

$$\frac{d\langle x_{ij}\rangle}{dt} = \left\langle \frac{L}{4}(1 - x_{ij}) \sum_{s=1}^{4} x_{ij}^{(s)} - D x_{ij} \right\rangle. \tag{6}$$

If we neglect correlations in (6) and assume that, for any pair of sites a and b, $\langle ab\rangle = \langle a\rangle\langle b\rangle$, we arrive at the spatial

mean-field model

$$\frac{d\langle x_{ij}\rangle}{dt} = \frac{L}{4}(1-\langle x_{ij}\rangle)\sum_{s=1}^{4}\left\langle x_{ij}^{(s)}\right\rangle - D\langle x_{ij}\rangle. \tag{7}$$

Figure 1(b) demonstrates that the mean-field model is not a very accurate representation of the average behavior of the stochastic process (compare dotted and thick solid lines).

To improve upon the mean-field approximation we note that (6) introduces terms of the form $\langle x_{ij}\, x_{i+1,j}\rangle$ and $\langle x_{ij}\, x_{i,j+1}\rangle$, which require new equations to describe their rate of change. These are

$$\frac{d\langle x_{ij}\, x_{i+1,j}\rangle}{dt} = \left\langle \frac{L}{4}(1-x_{ij})\sum_{s=1}^{4} x_{ij}^{(s)}\, x_{i+1,j} + \frac{L}{4}(1-x_{i+1,j}) \times \sum_{s=1}^{4} x_{i+1,j}^{(s)}\, x_{ij} - 2D x_{ij}\, x_{i+1,j}\right\rangle, \tag{8}$$

$$\frac{d\langle x_{ij}\, x_{i,j+1}\rangle}{dt} = \left\langle \frac{L}{4}(1-x_{ij})\sum_{s=1}^{4} x_{ij}^{(s)}\, x_{i,j+1} + \frac{L}{4}(1-x_{i,j+1}) \times \sum_{s=1}^{4} x_{i,j+1}^{(s)}\, x_{ij} - 2D x_{ij}\, x_{i,j+1}\right\rangle. \tag{9}$$

Equations (8) and (9) introduce terms of the form $\langle bc\rangle$ and $\langle abc\rangle$, where a, b, and c are sites in the grid that satisfy $\mathrm{dist}(a,b) = \mathrm{dist}(a,c) = 1$ and $\mathrm{dist}(b,c) = 2$. In principle, these new terms require additional equations that involve higher order moments. At some point, however, we need to cut off the process of adding equations and instead use approximations to obtain a closed system.

B. Spatially explicit decoupling approximations and the pair approximation

Before proceeding, we need to establish notation and some fundamental relations. First, note that for any triad of sites $\{a,b,c\}$ the following relation always holds: $\langle bc\rangle - \langle abc\rangle = P(b=1,\ a=0,\ c=1)$. Let P_{ijk} be defined by

$$\begin{aligned}
P_{ij1} &= P(x_{i-1,j}=1, \quad x_{ij}=0,\ x_{i+1,j}=1),\\
P_{ij2} &= P(x_{i,j-1}=1, \quad x_{ij}=0,\ x_{i,j+1}=1),\\
P_{ij3} &= P(x_{i-1,j}=1, \quad x_{ij}=0,\ x_{i,j-1}=1),\\
P_{ij4} &= P(x_{i,j-1}=1, \quad x_{ij}=0,\ x_{i+1,j}=1),\\
P_{ij5} &= P(x_{i+1,j}=1, \quad x_{ij}=0,\ x_{i,j+1}=1),\\
P_{ij6} &= P(x_{i-1,j}=1, \quad x_{ij}=0,\ x_{i,j+1}=1).
\end{aligned} \tag{10}$$

If we call $U_{ij} = \langle x_{ij}\rangle$, $Y_{ij1} = \langle x_{ij}\, x_{i+1,j}\rangle$, and $Y_{ij2} = \langle x_{ij}\, x_{i,j+1}\rangle$, then the system (6)–(9) can be rewritten succinctly as

$$\begin{aligned}
\dot{U}_{ij} &= \frac{L}{4}(U_{i-1,j} - Y_{i-1,j,1} + U_{i+1,j} - Y_{ij1} + U_{i,j-1} - Y_{i,j-1,2} + U_{i,j+1} - Y_{ij2}) - DU_{ij},\\
\dot{Y}_{ij1} &= \frac{L}{4}(U_{ij} + U_{i+1,j} - 2Y_{ij1} + P_{ij1} + P_{ij4} + P_{ij5} + P_{i+1,j,1} + P_{i+1,j,3} + P_{i+1,j,6}) - 2DY_{ij1},\\
\dot{Y}_{ij2} &= \frac{L}{4}(U_{ij} + U_{i,j+1} - 2Y_{ij2} + P_{ij2} + P_{ij5} + P_{ij6} + P_{i,j+1,2} + P_{i,j+1,3} + P_{i,j+1,4}) - 2DY_{ij2}.
\end{aligned} \tag{11}$$

The presence of the P_{ijk} in (11) means that this system is not closed. To close it, let us consider the following relations, where, as before $\mathrm{dist}(a,b) = \mathrm{dist}(a,c) = 1$, and $\mathrm{dist}(b,c) = 2$:

$$\begin{aligned}
P(b=1,a=0,c=1) &= P(b=1|a=0,c=1)P(a=0,\ c=1)\\
&\approx P(b=1|a=0)P(a=0,\ c=1)\\
&= (\langle b\rangle - \langle ab\rangle)/(1-\langle a\rangle)(\langle c\rangle - \langle ac\rangle).
\end{aligned} \tag{12}$$

Intuitively, the approximation $P(b|a=0,\ c=1) \approx P(b=1|a=0)$ assumes that the probability that a site is equal to one is only weakly dependent on the probability that another site two units of distance apart is also equal to 1. Now, let $\delta_{ij} = 1/(1-U_{ij})$ if $U_{ij} < 1$ and $\delta_{ij} = 0$ otherwise. If we define the B_{ijk} by

$$\begin{aligned}
B_{ij1} &= (U_{i+1,j} - Y_{ij1})(U_{i-1,j} - Y_{i-1,j,1}), \quad B_{ij2} = (U_{i,j-1} - Y_{i,j-1,2})(U_{i,j+1} - Y_{ij2}),\\
B_{ij3} &= (U_{i,j-1} - Y_{i,j-1,2})(U_{i-1,j} - Y_{i-1,j,1}), \quad B_{ij4} = (U_{i,j-1} - Y_{i,j-1,2})(U_{i+1,j} - Y_{ij1}),\\
B_{ij5} &= (U_{i+1,j} - Y_{ij1})(U_{i,j+1} - Y_{ij2}), \quad B_{ij6} = (U_{i-1,j} - Y_{i-1,j,1})(U_{i,j+1} - Y_{ij2}),
\end{aligned} \tag{13}$$

then, using (12), we arrive at the approximations $P_{ijk} \approx \delta_{ij}B_{ijk}$. We call these approximations *spatially explicit decoupling approximation*, or SEDA. Finally, substituting the P_{ijk} in (11) yields the following closed-form approximation for the system:

$$\begin{aligned}
\dot{U}_{ij} &= \frac{L}{4}[U_{i-1,j} - Y_{i-1,j,1} + U_{i+1,j} - Y_{ij1} + U_{i,j-1} - Y_{i,j-1,2} + U_{i,j+1} - Y_{ij2}] - DU_{ij},\\
\dot{Y}_{ij1} &= \frac{L}{4}[U_{ij} + U_{i+1,j} - 2Y_{ij1} + \delta_{ij}(B_{ij1} + B_{ij4} + B_{ij5}) + \delta_{i+1,j}(B_{i+1,j,1} + B_{i+1,j,3} + B_{i+1,j,6})] - 2DY_{ij1},\\
\dot{Y}_{ij2} &= \frac{L}{4}[U_{ij} + U_{i,j+1} - 2Y_{ij2} + \delta_{ij}(B_{ij2} + B_{ij5} + B_{ij6}) + \delta_{i,j+1}(B_{i,j+1,2} + B_{i,j+1,3} + B_{i,j+1,4})] - 2DY_{ij2}.
\end{aligned} \tag{14}$$

System (14) preserves information of neighbors up to one unit of distance apart in the ℓ_1 metric, for this reason we refer to this model as first-order SEDA. Similarly, using the same type of approximation, we can construct a model that preserves correlations of neighbors that lie up n units of distance apart from each other; we refer to this model as nth-order SEDA. Note that throughout this paper, when we make reference to a SEDA approximation without specifying the order, we are referring to a first-order approximation. In the Supplemental Material (SM) [27] we give general rules for higher order SEDA and present the formulas for second order, which requires 24 differential equations per point [instead of the just three required in (14)].

We can recover the traditional so called *pair approximations* (PA) from the first-order SEDA equations (14). To do so, let us first define U as the total number of individuals, N as the number of sites in the grid, and Y as the average correlation between any two nearest neighbors times N. To derive the PA equations from (14) we need to (i) set the $\delta_{ij} = 1$, which in SEDA prevent singularities at individual sites; (ii) assume spatial homogeneity, that is, $U = NU_{ij}$ and $Y = NY_{ij1}$ for any (i, j); and (iii) set $Y_{ij2} = Y_{ij1}$. The PA equations for the birth-death process are

$$\begin{aligned}\dot{U} &= L(U - Y) - DU,\\ \dot{Y} &= \frac{L}{2}(U - Y) + \frac{3L}{2}(U - Y)^2/(N - U) - 2D. \end{aligned} \quad (15)$$

We remark on two key differences between PA and SEDA: (1) PA models are nonspatial. They track only the total number of individuals, but not the spatial location of each individual. (2) PA models only consider correlations of pairs, while, depending on the order, SEDA models can preserve correlations for larger groups of neighbors (e.g., up to quintuplets in second-order equations).

Figure 1(b) plots the expected number of individuals as a function of time, calculated from stochastic simulations, the mean-field model, first- and second-order SEDA, and PA. It is clear from this figure that first-order SEDA is closer to the results from the stochastic process than the PA or mean-field models. We also see that second order improves on the first-order approximation, but the agreement with the stochastic results is still far from optimal. In Sec. III, we will build on first-order SEDA to find more accurate deterministic representations of the expected behavior of the stochastic process.

III. RADIAL DECOUPLING, TRIGONOMETRIC APPROXIMATIONS, AND TIME-SCALING SEDA

In this section we provide methods to improve the SEDA description of range expansion, to reach nearly perfect approximations in a wide range of parameters. We first develop a new approximation, which we call radial decoupling approximation. We then combine this radial approximation with SEDA, to find a method that produces much better agreement with the stochastic process than pure SEDA alone. We call this combined method trigonometric decoupling approximation. Finally, we introduce an alternative, time-scaling approach that also improves SEDA results.

A. Radial decoupling approximations

In Sec. II B, we used approximation (12) for quantity $\mathcal{P}_{abc} = P(b = 1,\ a = 0,\ c = 1)$, where a, b, and c are sites in the grid, that satisfy $\text{dist}(a, b) = \text{dist}(a, c) = 1$ and $\text{dist}(b, c) = 2$ (note that subindexes in $\mathcal{P}_{abc}$ are sites and not coordinates). Here, we develop a different approximation for this quantity. We focus on modeling 2D growth expanding radially from an origin o, with coordinates (i_o, j_o).

We begin by noting the following relations:

$$\mathcal{P}_{abc} = P(b = 1|a = 0,\ c = 1)P(a = 0,\ c = 1) \quad (16)$$

$$= P(c = 1|a = 0,\ b = 1)P(a = 0,\ b = 1). \quad (17)$$

Numerical simulations show that, as time proceeds, soon after $\mathcal{P}_{abc}$ increases from its initial zero value, $P(b = 1|a = 0,\ c = 1)$ or $P(c = 1|a = 0,\ b = 1)$ remains relatively stable. Then, given that $P(a = 0,\ b = 1) = \langle b\rangle - \langle ab\rangle$ and $P(a = 0,\ c = 1) = \langle c\rangle - \langle ac\rangle$, the previous observation and Eqs. (16) and (17) suggest the approximations $\mathcal{P}_{abc} \approx \eta(\langle c\rangle - \langle ac\rangle)$ or $\mathcal{P}_{abc} \approx \eta(\langle b\rangle - \langle ab\rangle)$, where η is the stationary value for $P(c = 1|a = 0,\ b = 1)$ and $P(b = 1|a = 0,\ c = 1)$ (i.e., for time t large). We call these approximations *radial decoupling approximations*, or RDA.

We now describe a procedure to decide which of the two approximations [$\mathcal{P}_{abc} \approx \eta(\langle c\rangle - \langle ac\rangle)$ or $\mathcal{P}_{abc} \approx \eta(\langle b\rangle - \langle ab\rangle)$] to use, based on the geometry of the triad $\{a, b, c\}$ and the location of a relative to the origin o. First, we can think of a [with coordinates (i_a, j_a)] as the center of the triad. There is a unique line ℓ that goes through a and is perpendicular to the vector $\vec{bc}$; see Fig. 2. This line divides the plane into two half-planes: H_b, which contains the site b, and H_c, which contains the site c. Let v_a be the vector that goes from a to the site with coordinates $(i_a, j_a + 1)$. We can then define θ_{abc} as the angle between v_a and ℓ measured in a counterclockwise direction. Given the geometry of the grid, θ_{abc} will take on one the values $\pi/4, \pi/2, 3\pi/4$, or π (Fig. 2). If we measure angles based on the interval $[0,\ 2\pi)$, one of the half-planes discussed will be made up of those sites e where the angle from v_a to $\vec{ae}$ (measured counterclockwise) lies between θ_{abc} and $\theta_{abc} + \pi$. To simplify the notation let us assume that this half-plane is H_b. Now, let v_o be the vector from o to the site with coordinates $(i_o, j_o + 1)$. If the angle θ_{oa} from v_o to $\vec{oa}$ is such that $\theta_{abc} \leqslant \theta_{oa} < \theta_{abc} + \pi$, use the approximation $\mathcal{P}_{abc} \approx \eta(\langle b\rangle - \langle ab\rangle)$; otherwise, use $\mathcal{P}_{abc} \approx \eta(\langle c\rangle - \langle ac\rangle)$. To further simplify the notation, in the future we will also refer to θ_{oa} as θ_{ij}.

The procedure/algorithm described in the previous paragraph is informed by simulation results. The critical time to model $\mathcal{P}_{abc}$ is during the transitional time period where this quantity changes from a near zero state to its long term stationary value. During this transitional period, the triad $\{a, b, c\}$ is located near the edge of the radially expanding population. Simulation results indicate that the best RDA is the one that explicitly tracks information from the site (either b or c) that is most likely to lie outside the radially expanding population during this transitional time. Intuitively this makes sense. This is because the expected value of a site that lies outside the expanding population is more likely to change during this time than the expected value of a site that lies inside the population mass, where it is more likely to be

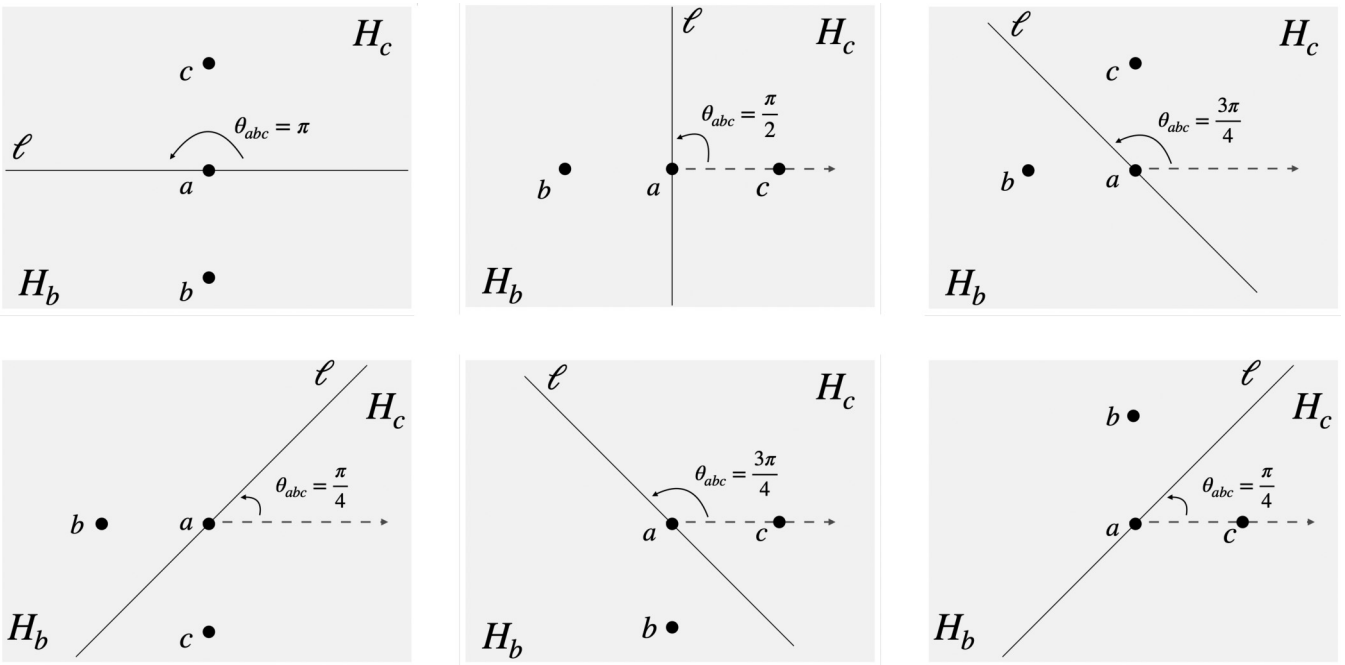

FIG. 2. Panels show all geometric configurations for sites a, b, and c that satisfy $\mathrm{dist}(a, b) = \mathrm{dist}(a, c) = 1$ and $\mathrm{dist}(b, c) = 2$. Clockwise from top right, the configurations describe the sites in the probabilities P_{ijk} from $k = 1, \ldots, 6$ [Eq. (10)]. The angles and semiplanes (θ_{abc}, H_b, and H_c) are used to determined which RDA approximation to use, $\eta(\langle b\rangle - \langle ab\rangle)$ or $\eta(\langle c\rangle - \langle ac\rangle)$, based on the location of a relative to the population origin o. See text for discussion and Table I.

near its long term steady-state. The algorithm described in the previous paragraph selects the best RDA according to this criterion.

Table I specifies how to choose the RDA for the P_{ijk} in (10). Following the definitions of the A_{ijk} in this table, the approximations can be written succinctly as $P_{ijk} \approx \eta A_{ijk}$. A closed-form approximation for system (11) then follows by substituting the P_{ijk} by ηA_{ijk} in (11). We can determine η by considering the equations of the new system at equilibrium. We do so by setting the equations equal to zero, dropping the subscripts, and solving for η. We find $\eta = 1 - \frac{4D}{3L}$, which suggests a valid approximation for $D/L < 0.75$. This equilibrium analysis, however, also reveals that, unlike the stochastic process, a system based only on RDA does not have a unique nontrivial steady state. Instead, we discover that combining RDA with SEDA restores a unique equilibrium to the system and provides very accurate results. We discuss this combined approach next.

B. Trigonometric approximation

Before we proceed we can introduce a small correction by modifying the SEDA model so that its steady-state density more closely matches that of the corresponding stochastic process. The procedure consists of substituting the approximation $P_{ijk} \approx \delta_{ij} B_{ijk}$ by $P_{ijk} \approx \min(\epsilon \delta_{ij} B_{ijk}, 1)$, where $\epsilon \geqslant 1$. Using the notation of Sec III A, this implies that on average $P(b = 1|a = 0,\ c = 1) \geqslant P(b = 1|a = 0)$. This intuitively makes sense because, being at most two units of distance apart from each other, the values of b and c are correlated. To determine ϵ, we can substitute the steady-state densities of the stochastic process, U_s and Y_s, with the modified approximations for P_{ijk} into (14), set these equations equal to zero, and solve for ϵ; this yields

$$\epsilon = \left(\frac{L}{D} - \frac{4}{3}\right)(1 - U_s)U_s^{-1}. \tag{18}$$

TABLE I. Columns 1 to 4: Radial decoupling approximation, A_{ijk}, of P_{ijk}, based on the angle θ_{oa} from v_o to $\vec{oa}$ (see text). Columns 1 and 5: Trigonometric coefficients α_{ijk} for each P_{ijk}. Note that $\theta_{oa} = \theta_{ij}$ (same angle, different notation).

$\mathcal{P}_{abc}$	θ_{abc}	$\theta_{oa} \in [\theta_{abc}, \theta_{abc} + \pi)$	$\theta_{oa} \notin [\theta_{abc}, \theta_{abc} + \pi)$	α_{ijk}
P_{ij1}	π	$A_{ij1} = U_{i+1,j} - Y_{ij1}$	$A_{ij1} = U_{i-1,j} - Y_{i-1,j,1}$	$c_{\cos}\cos(2\theta_{ij}) + m_{\cos}$
P_{ij2}	$\pi/2$	$A_{ij2} = U_{i,j-1} - Y_{i,j-1,2}$	$A_{ij2} = U_{i,j+1} - Y_{ij2}$	$-c_{\cos}\cos(2\theta_{ij}) + m_{\cos}$
P_{ij3}	$3\pi/4$	$A_{ij3} = U_{i,j-1} - Y_{i,j-1,2}$	$A_{ij3} = U_{i-1,j} - Y_{i-1,j,1}$	$-c_{\sin}\sin(2\theta_{ij}) + m_{\sin}$
P_{ij4}	$\pi/4$	$A_{ij4} = U_{i,j-1} - Y_{i,j-1,2}$	$A_{ij4} = U_{i+1,j} - Y_{ij1}$	$c_{\sin}\sin(2\theta_{ij}) + m_{\sin}$
P_{ij5}	$3\pi/4$	$A_{ij5} = U_{i+1,j} - Y_{ij1}$	$A_{ij5} = U_{i,j+1} - Y_{ij2}$	$-c_{\sin}\sin(2\theta_{ij}) + m_{\sin}$
P_{ij6}	$\pi/4$	$A_{ij6} = U_{i-1,j} - Y_{i-1,j,1}$	$A_{ij6} = U_{i,j+1} - Y_{ij2}$	$c_{\sin}\sin(2\theta_{ij}) + m_{\sin}$

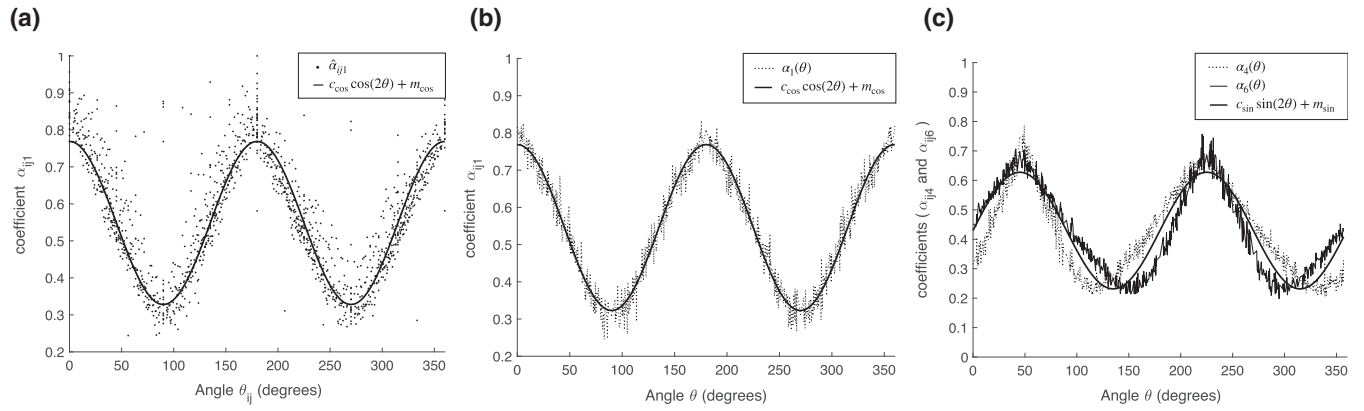

FIG. 3. Weight coefficients for the trigonometric approximation. (a) Best fit coefficients $\hat{\alpha}_{ij1}$ vs the angles θ_{ij} for each site in the grid (scattered plot); trigonometric approximation (solid line). (b) $\alpha_1(\theta)$ is the average of all $\hat{\alpha}_{ij1}$, for which $\theta_{ij}=\theta$ (dotted line). (c) $\alpha_4(\theta)$ and $\alpha_6(\theta)$ (dotted and thin lines); trigonometric approximation (thick line). $D=0.1$; $L=4$; grid size 45×45. For the behavior of the other weight coefficients ($\alpha_{ij2}, \alpha_{ij3}, \alpha_{ij5}$) see Table I.

Note that U_s and Y_s are independent of grid size. Hence, using (18), for any ratio D/L we can compute the value of ϵ from simulations in a small grid. After calculating several of these values, we can find a formula for ϵ using polynomial regression (see Fig. A2 in the SM [27]):

$$\epsilon = 1.85(D/L)^3 - 0.46(D/L)^2 + 0.045(D/L) + 1 \quad (19)$$

We now introduce a method to combine SEDA and RDA for the probabilities P_{ijk}. One approach is to weight the two types of approximations and add them up. More precisely, letting $\alpha_{ijk}\in[0,1]$, we consider approximations of the form

$$P_{ijk}\approx C_{ijk}=\alpha_{ijk}\underbrace{\min(\epsilon\,\delta_{ij}B_{ijk},1)}_{\text{SEDA}}+(1-\alpha_{ijk})\underbrace{(1-\tfrac{4D}{3L})A_{ijk}}_{\text{RDA}}. \quad (20)$$

Next, we need to determine appropriate values for the weights α_{ijk}. We begin by exploring the problem numerically, with a focus on modeling 2D growth expanding radially from an origin o. For a given grid size and set of parameters D and L, we can run multiple simulations past the point where the system reaches its stationary distribution. From these simulations we can compute the statistics (known as sample statistics) $\overline{P}_{ijk}(t)$, $\overline{\delta_{ij}B}_{ijk}(t)$, and $\overline{A}_{ijk}(t)$. We can then define $\hat{\alpha}_{ijk}$ as the parameter $\alpha_{ijk}\in[0,1]$ that minimizes $||\overline{P}_{ijk}(t)-\{\alpha_{ijk}\min[\epsilon\overline{\delta_{ij}B}_{ijk}(t),1]+(1-\alpha_{ijk})(1-\frac{4D}{3L})\overline{A}_{ijk}(t)\}||_{\ell_1}$. Intuitively, $\hat{\alpha}_{ijk}$ provides the best approximation possible for P_{ijk} that uses Eq. (20). Figure A4 in the SM [27] shows that these "best fit" combined approximations (i.e., using the $\hat{\alpha}_{ijk}$) provide a significant improvement over the pure SEDA approximations. Figure 3(a) plots the coefficients $\hat{\alpha}_{ij1}$ vs the angles θ_{ij} (dots). The plot shows that the coefficients are approximately periodic with the angles, which suggests that we could use a trigonometric formula for the α_{ij1}. Indeed, the black curve in this figure is the function $c_{\cos}\cos(2\theta)+m_{\cos}$. To determine the parameters $c_{\cos}$ and $m_{\cos}$, we average the $\hat{\alpha}_{ij1}$ that have the same θ_{ij}; for a given angle θ let this average be $\alpha_1(\theta)$. We then use a basic optimization procedure to find the parameters $c_{\cos}$ and $m_{\cos}$ that minimize $||\alpha_1(\theta)-[c_{\cos}\cos(2\theta)+m_{\cos}]||_{\ell_1}$ [Fig. 3(b)]. Similarly, Fig. 3(c) plots the averages $\alpha_4(\theta)$ and $\alpha_6(\theta)$ computed from the coefficients $\hat{\alpha}_{ij4}$ and $\hat{\alpha}_{ij6}$. In this case, the trigonometric formula for the α_{ij4} and α_{ij6} has the form $c_{\sin}\sin(2\theta_{ij})+m_{\sin}$ (thick line). Note here that the fitting of α_4 and α_6 would not benefit from a phase shift, because the error data do not exhibit the same symmetry as the sine function does. Instead, the sine approximation mostly lies between α_4 and α_6. However, since α_4 and α_6 appear in tandem in the ODEs, the net effect will produce an overall very good fit. We find then that the formulas for the six coefficients α_{ijk} ($k=1,\ldots,6$), can be expressed in terms of four parameters, $c_{\cos}, m_{\cos}, c_{\sin}$, and $m_{\sin}$, as described by Table I. We call the approximations that use the α_{ijk} in this table *trigonometric decoupling approximation*, or TDA. Compared to SEDA, TDA produce significantly smaller errors approximating the probabilities P_{ijk} (Fig. A5 in the SM [27]).

Finally, Fig. 4 plots the expected number of individuals as a function of time. In each panel stochastic simulations are compared to results from the mean-field model, SEDA, and TDA, for different death rates and grid sizes. In this figure the trigonometric approximation improves with grid size. This behavior is caused by the periodic boundary conditions used in the simulations, which are not specifically accounted for in the formulas for the α_{ijk}. Hence, as the grid size increases and the contribution of the boundary effects to the overall population diminishes, the trigonometric approximation improves. We see this in Fig. 4: once grid size is sufficiently large, the agreement between the TDA model and simulation results is excellent.

We calculated the coefficients $c_{\cos}, m_{\cos}, c_{\sin}, m_{\sin}$ for different values of D/L and then fitted the data with polynomial functions (Fig. A3 in the SM [27]) using least-squares in grids of size 45×45; these polynomial regressions yield the equations

$$\begin{aligned} c_{\cos} &= 0.39(D/L)^2 - 0.46(D/L) + 0.24,\\ c_{\sin} &= -2.4(D/L)^3 + 2.1(D/L)^2 - 0.72(D/L) + 0.22,\\ m_{\cos} &= -9.7(D/L)^3 + 7.5(D/L)^2 - 2(D/L) + 0.59,\\ m_{\sin} &= -8.6(D/L)^3 + 5.3(D/L)^2 - 1.4(D/L) + 0.46, \end{aligned} \quad (21)$$

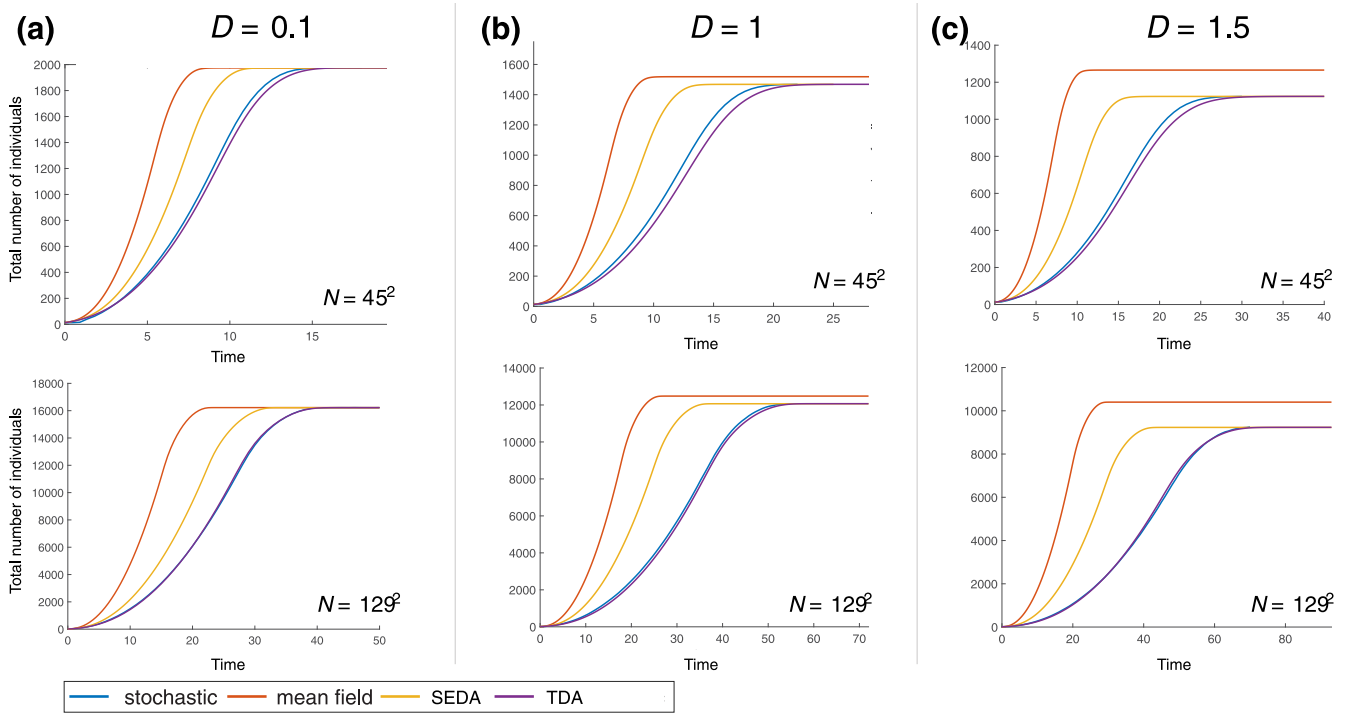

FIG. 4. Expected total number of individuals as a function of time. Stochastic simulation results (blue) compared with the output of three deterministic models: mean field (red), SEDA (yellow), and TDA (purple). For all plots the reproduction rate $L = 4$. The death rates are (a) $D = 0.1$, (c), (b) $D = 1$, and (c) $D = 1.5$. Grid sizes indicated in bottom-right corner of each panel ($N = 45^2$ or $N = 129^2$). Stochastic results based on at least 10^4 independent simulations per curve (error bars smaller than thickness of curves, not shown).

$$\begin{aligned}
\dot{U}_{ij} &= \frac{L}{4}(U_{i-1,j} - Y_{i-1,j,1} + U_{i+1,j} - Y_{ij1} + U_{i,j-1} - Y_{i,j-1,2} \\
&\quad + U_{i,j+1} - Y_{ij2}) - DU_{ij}, \\
\dot{Y}_{ij1} &= \frac{L}{4}(U_{ij} + U_{i+1,j} - 2Y_{ij1} + C_{ij1} + C_{ij4} + C_{ij5} + C_{i+1,j,1} \\
&\quad + C_{i+1,j,3} + C_{i+1,j,6}) - 2DY_{ij1}, \\
\dot{Y}_{ij2} &= \frac{L}{4}(U_{ij} + U_{i,j+1} - 2Y_{ij2} + C_{ij2} + C_{ij5} + C_{ij6} \\
&\quad + C_{i,j+1,2} + C_{i,j+1,3} + C_{i,j+1,4}) - 2DY_{ij2},
\end{aligned} \tag{22}$$

and their validity was verified for grids roughly 8, 500, and 5000 times larger (Figs. 4 and 6). Together Eqs. (13) and (20)–(22) and Table I provide a full and explicit formula for the TDA model. This approximation is very successful for $D/L \leqslant 0.4$, which roughly corresponds to steady-state densities $\geqslant 50\%$.

C. Time-scaling SEDA

For each grid site (i, j) there is a transient time period where the values of the approximations $\delta_{ijk}B_{ijk} < P_{ijk}$ (compare blue and yellow lines in Fig. A4 in the SM [27]). During this time period, the derivative of U_{ij} calculated using SEDA is larger than the same derivative according to the stochastic process. As a consequence, before reaching the steady state, system (14) overestimates the total number of individuals as a function of time (Figs. 1 and 4). Heuristically, these observations suggest that, by scaling time by a parameter $\alpha_{D/L} \leqslant 1$ in (14), we can improve the quality of the approximation. More precisely if S is the total number of individuals and (14) yields the functional relation $S = F(t)$, then we can improve the approximation by setting $S = F(\alpha_{D/L}t)$, where the value of $\alpha_{D/L}$ is determined through least-squares fitting in a small grid (Fig. 5). We can then find through polynomial regression a formula for $\alpha_{D/L}$ valid for $D/L \leqslant 0.4$:

$$\alpha_{D/L} = (1.72(D/L)^2 + 0.0795(D/L) + 1.3)^{-1} \tag{23}$$

We tested Eqs. (21) for the trigonometric parameters and (23) for the $\alpha_{D/L}$ in much larger grids (Fig. 6). As initial conditions we used random plaques grown stochastically from an initial set of 13 occupied sites at the center of the grid (left image of each panel). Here the sizes of the initial plaques are large enough so that with them as initial conditions the trajectories of the total number of individuals as a function time behave almost deterministically; hence, a single stochastic run is sufficient to track the time evolution of the expected number of individuals. We find that (21) and (23) produce very good approximations, in much larger grids with random plaques as initial conditions.

Next, we discuss the numerical solution of the approximate systems. These systems of course can be solved using higher order implicit methods, such as Runge-Kutta, which is the standard method, and unless stated otherwise is behind the figures in the paper. However, we are interested in evaluating the performance and accuracy of forward Euler, as this method is the simplest to implement and fastest to compute. We found that in forward Euler a step size of $dt = 0.025L$ provides good results for $0.25 \leqslant D/L \leqslant 0.4$ and a step size of $dt = 0.0125L$ is sufficient for all $D/L \leqslant 0.4$. The approximate systems yield

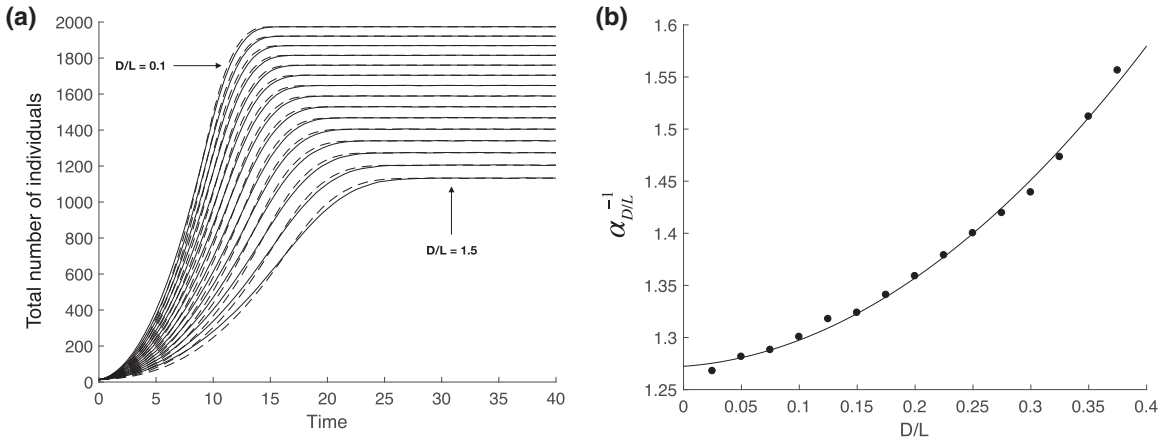

FIG. 5. Time-scaled SEDA. (a) Solid lines show the trajectories of the expected number of individuals as a function of time calculated from 5000 independent simulations per curve (error bars too small to plot). Dashed lines show time-scaled SEDA. (b) Inverse of time-scaling parameter, $\alpha_{D/L}^{-1}$, as a function of D/L. Curve plots the polynomial regression in Eq. (23) (adjusted coefficient of determination $\bar{R}^2 > 0.99$). In all simulations $L = 4$ and grid size is 45×45.

very large improvements in computational performance compared to stochastic simulations for large grids. For example, for the simulations in Fig. 6(b), with a grid size of $\approx 10^7$ sites, and a death-to-birth ratio $D/L = 0.25$, before reaching saturation the trigonometric approximation was more than 100 times faster than a single stochastic run.

Finally, we note that applying the rescaling procedures described in this section to PA or the spatial mean-field model does not produce satisfactorily results (Sec. F in the SM [27]). Indeed, besides PA being nonspatial, the curve shapes of a rescaled PA and the stochastic results are substantially different (Fig. A8 in the SM [27]). Also, rescaling the spatial mean-field model easily results in high relative errors and very inaccurate approximations to the stochastic process at early times t (Fig. A9 in the SM [27]).

IV. STEADY-STATE DENSITY

Here we focus on the steady-state behavior of the spatial birth death process, and derive several approximations for the steady-state density. We note that up to this point we have only dealt with von Neumann neighborhoods. In this and the next section we also consider Moore neighborhoods in relation to both steady-state and range expansion results. For a derivation of the steady-state formulas in 3D see SM Sec. G [27].

A. Steady-state density for the von Neumann neighborhood

As seen from the long term dynamics in Fig. 1(b), in a finite grid, the expected population size eventually reaches a steady state. We can calculate the steady-state density predicted by the mean-field approximation by dropping the subscripts in (7) and setting the right-hand side of the equation to zero. Solving this equation, we find that the steady-state density in the mean-field model is equal to that of mass action [formula (1)]. Here mass action refers to the well-mixed nonspatial version of the birth-death process, described by equation $\dot{X} = LX(1 - X/K) - DX$, where X is the total number of individuals, K the system's carrying capacity, and $\rho_{ma} = X/K$ in steady state.

For the stochastic process, what we call here the steady-state (or equilibrium) density refers to the expected density of the quasistationary distribution calculated from simulations [28]. During simulations, if early extinction is avoided, the

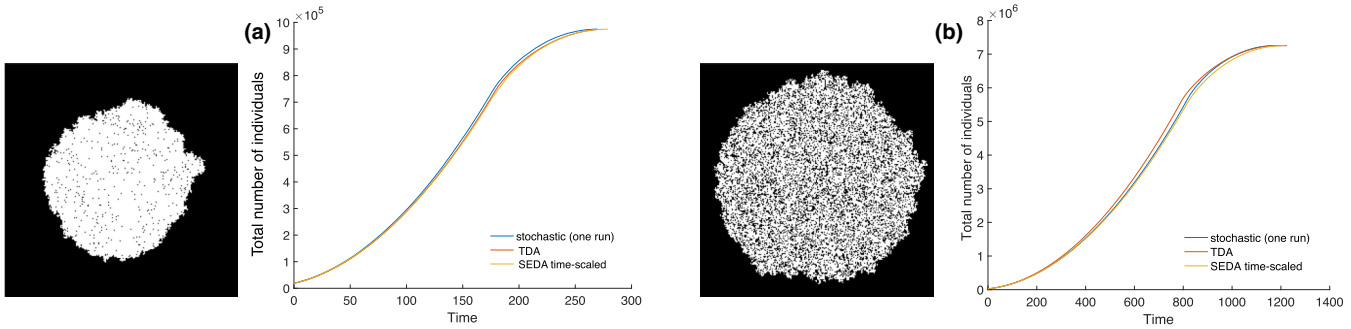

FIG. 6. Expected number of individuals as a function of time in large grids. The initial conditions (random plaques) are shown on the left side of each panel (occupied sites are depicted in white, empty sites in black). (a) Death rate $D = 0.1$, grid size 1000×1000, 18 000 occupied sites at $t = 0$ (1.8% of grid size). (b) Death rate $D = 1$, grid size 3163×3163, 25 000 occupied sites at $t = 0$ (0.25% of grid size). In both panels the reproduction rate $L = 4$.

expected number of individuals eventually plateaus and then remains stable during the remainder of the simulated time. The steady-state density is taken from this plateau value. The first thing we note is that the mean-field approximation provides a poor representation of the stochastic equilibrium density [Fig. 1(c), dotted line]. Applying the same procedure to (14), and noting that when the system is at equilibrium $Y_{ij1} = Y_{ij2}$ [or solving system (15) in steady state], we find the equilibrium density for the PA and first-order SEDA models to be given by formula (2). In Fig. 1(c) we see that (2) provides very good agreement with the steady-state densities from the stochastic process (for densities larger than 50%). Also, we again notice that the second order improves slightly over the first-order approximation (especially at lower densities).

Finally, we note that when the initial number of individuals, n_0, is small, extinction events can be caused by random fluctuations around small numbers. Indeed, the probability of early extinction is at least $[D/(D+L)]^{n_0}$. However, unless n_0 is quite small, there are parameter regions where early extinction is very unlikely. In particular, during simulations for Fig. 1(c), extinction never occurred for all points that were tested with $D/L < 0.62$ ($n_0 = 13$). For $D/L \geqslant 0.62$ on the other hand, population extinction always occurred, even when simulations started with a completely full grid. (For more on extinction from low numbers see [29,30].)

B. Steady-state density for the Moore neighborhood

Moore neighborhoods can be defined in terms of the ℓ_∞ distance, which states that $\text{dist}(x_{ij}, x_{lk}) = \max(|i-l|, |j-k|)$. The Moore neighborhood of radius 1 of a site a can then be described as a and all sites that lie one unit of distance apart from a (eight neighbors in total). When dealing with Moore neighborhoods, in addition to the variables $Y_{ij1} = \langle x_{ij}x_{i,j+1}\rangle$ and $Y_{ij2} = \langle x_{ij}x_{i,j+1}\rangle$, it useful to introduce the quantities $Y_{ij3} = \langle x_{ij}x_{i-1,j+1}\rangle$ and $Y_{ij4} = \langle x_{ij}x_{i+1,j+1}\rangle$. We can then use these variables to approximate the steady-state density of the system. Following the general methodology employed in the paper, we begin by writing ODEs for the rate of change of the variables $U_{ij} = \langle x_{ij}\rangle$, Y_{ij1}, Y_{ij2}, Y_{ij3}, and Y_{ij4}. The resulting equations include objects of type $P(b=1, a=0, c=1)$, where b and c are two distinct sites in the Moore neighborhood of radius 1 of a third site a. To proceed in the same way as for the von Neumann model, we apply the approximation in Eq. (12) to all triplets with $\text{dist}(b,c) = 2$. As a result, new variables must be added to the system. After symmetrizing for the steady-state analysis, we obtain a system of five equations [instead of the two for the von Neumann case (15)]. We present and solve these equations numerically in SM Sec. E [27].

There is, however, a way to simplify the equations that allows for an analytical solution. Given a triplet, $\{a, b, c\}$, that satisfies the conditions previously described, we can apply approximation (12) *regardless* of the distance separating b and c. This approach leads directly to a closed system of ODEs. As before, to perform the steady-state analysis, we drop the coordinate subscripts for all variables in the system, and find that the steady-state values for Y_1, Y_2, Y_3, and Y_4 are all the same. Simply calling this steady state Y leads to the equilibrium equations[1]

$$0 = L(U-Y) - DU,$$
$$0 = \tfrac{7}{4}L(U-Y)^2/(1-U) + \tfrac{1}{4}L(U-Y) - 2DY. \quad (24)$$

Solving this last system for U, we find the closed-form approximation for the Moore neighborhood equilibrium density (4). This formula fits the numerically obtained data remarkably well (see SM Fig. A7 [27]), and is only slightly less accurate than the more cumbersome method of decoupling used in SM Sec. E [27]. This same simplifying approach can be used to find an approximation, ρ_H, for the steady-state density in a hexagonal (honeycomb) lattice, where each node has six nearest neighbors; see formula (3). The order relation between the approximate densities, $\rho_{vN} \leqslant \rho_H \leqslant \rho_M$, reflects what occurs in stochastic simulations, where the steady-state density increases with the number of neighbors.

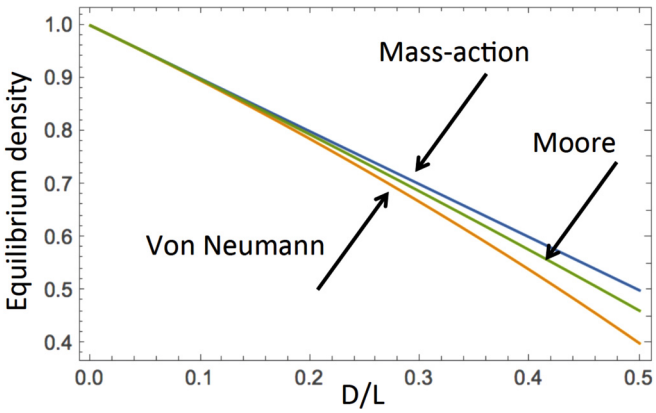

FIG. 7. The equilibrium density in mass-action (mean-field), von Neumann, and Moore models, as functions of the death-to-divisions ration. The lines correspond to formulas (1), (2), and (4).

Figure 7 plots the equilibrium density formulas for the mass-action, von Neumann, and Moore models. As we noted, spatial restrictions reduce the equilibrium density. In this sense, the von Neumann model imposes stronger spatial restrictions than the Moore model (four vs eight nearest neighbors per site). The corresponding equilibrium density is therefore lower in the von Neumann model. It is important to note that formulas (2) and (4) capture this behavior, while the mean-field representations do not. Indeed, although the mass-action model and the spatial mean-field models for von Neumann [Eq. (7)] and Moore (not shown) have different propagation speeds, they all have the same steady-state density.

V. POPULATION EXPANSION RATE

In this section we are interested in approximating the expected growth rate of a 2D population expanding radially from an origin o in an infinite grid. Under these conditions, when the population is large enough, the region of the grid colonized by the population up to a time t will roughly resemble a disk

[1]Note that if we use this simplification for the von Neumann neighborhood, we recover first-order SEDA.

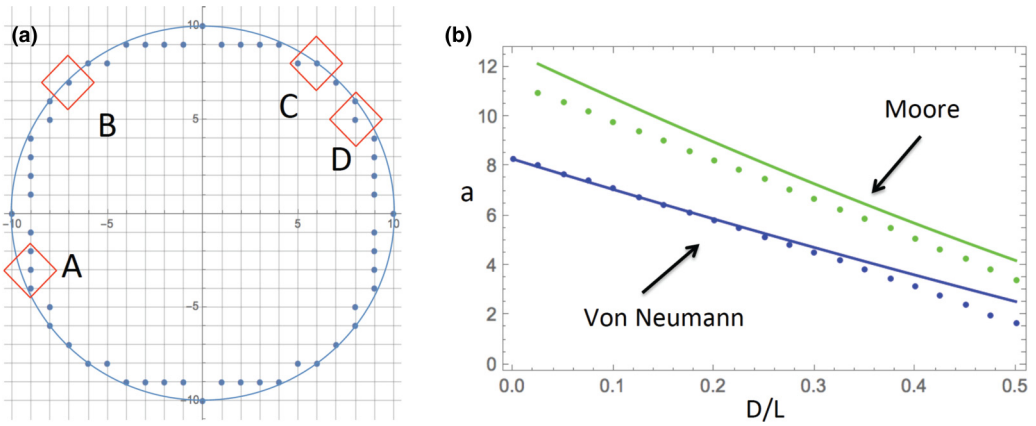

FIG. 8. (a) Surface points of a circular domain on a square grid. Calculations are demonstrated for the von Neumann model. For point A, two of its neighbors belong to the surface and one neighbor lies outside the circle. For point B, two neighbors are in the interim, and two lie outside the circle. For point C, one of the neighbors is part of the surface set and two lie outside the circle. For point D, one neighbor is part of the surface set and one lies outside the surface. (b) Growth rate parameter a as a function of D/L [Eq. (27)] for $L = 4$, for von Neumann and Moore neighborhood models. Calculated from stochastic simulations (dots) and formulas (solid lines).

(see, for example, initial conditions in Fig. 6). It is possible to derive approximate expressions for the expansion rate of these disks, as colonization proceeds.

Let $A(t)$ be the area of the expanding region and $M(t)$ the total number of occupied sites. In the region's interior the density of occupied sites will be near equilibrium and thus we will have the relation $M(t) \approx A(t)\rho$, where ρ is the steady-state density of occupied sites. We can then define the radius R and circumference C of the disk-like region in terms of M:

$$A = \pi R^2, \quad C = 2\pi R = 2\sqrt{\pi A} \approx 2\sqrt{\frac{\pi M}{\rho}}. \tag{25}$$

In the colonized region's interior, divisions exactly balance deaths; the number of individuals only increases through the dynamics on its boundary or surface, where there is no such balance. For this reason, we want to estimate the number of surface sites of a disk-like region. Let us begin by considering a circle of radius r and center o with coordinates (i_o, j_o) in a rectangular grid. We define the surface points of the circle as those with coordinates (i, j) such that (i) $(i - i_o)^2 + (j - j_o)^2 \leqslant r^2$ and (ii) the point has at least one nearest neighbor, (i_1, j_1), that lies outside of the circle, i.e., $(i_1 - i_o)^2 + (j_1 - j_o)^2 > r^2$. Such points are denoted as blue dots in Fig. 8(a), which illustrates this for the von Neumann neighborhood. We find numerically that for large r the number of sites in the circle's surface $\approx \beta \times 2\pi r$, where β is constant that depends on the type of neighborhood used. Hence by analogy, we estimate that the number of surface sites, $S(t)$, of a stochastic disk-like region is

$$S \approx \beta \times 2\pi R \approx \beta \times 2\sqrt{\frac{\pi M}{\rho}}. \tag{26}$$

We are only interested in the dynamics at the surface, where the approximate number of individuals is $S\rho$. The net growth rate of the system is $L - D$; however, at the surface only the fraction of the growth rate directed towards the outside of the disk, ν, counts towards expansion. The other fraction of the surface growth, $1 - \nu$, is directed towards the interior of the disk-like region, where we assume that births and deaths are balanced. This fraction, ν, is equal to the average number of exterior and surface neighbors that an individual at the surface has, divided by 4. The approximate total growth rate is then equal to $\nu(L - D)\rho S$, where the inclusion of $\sqrt{\rho}$ introduces a nonlinear term. The equation for the total population can be written as

$$\frac{dM}{dt} = \nu\rho S(L - D) = \nu\beta \times 2\sqrt{\pi\rho M}(L - D) = a\sqrt{M}, \tag{27}$$

where the expansion rate a is given by

$$a = 2\nu\beta\sqrt{\pi\rho}\ \ (L - D), \tag{28}$$

and quantities ν, ρ, and β depend on the type of neighborhood used. The expansion rate in (28) was derived from first principles, where all components have a physical meaning. It is worth mentioning, however, that a simple linear regression of the data in Fig. 8 would result in a tighter fit for a.

A. Expansion rate for the von Neumann neighborhood

Using the von Neumann model, we can numerically estimate the number of surface points in a circle of a given radius, which leads to the value $\beta_{vN} \approx 0.9$; see Fig. 8(a). The density formula is given by Eq. (2).

The next step in our derivation is to find an estimate for ν_{vN}. Let us begin again by considering a circle. For each point in a circle's surface, we want to determine how many of its four nearest neighbors lie outside the circle, belong to its surface, or belong to the circle's interior. In Fig. 8(a) a circle's surface points are marked as blue dots; for illustrations purposes, the neighbors of four of these points (A, B, C, and D) are enclosed in red diamonds. For point A, two of its neighbors belong to the surface and one neighbor lies outside the circle. For point B, two neighbors are in the interior and two lie outside the circle. For point C, one neighbor is in the surface and two lie outside the circle. For point D, one neighbor is in the surface

and one lies outside. Hence, for points A and C, three out of their four neighbors are not in the interior. For points B and D, two of their neighbors are not in the interior. Increasing the circle's radius and calculating the average fraction of neighbors that lie either outside the circle or in its surface, we find numerically that this quantity, $\nu_{vN} \approx 0.65$. Figure 8(b) plots the values of the growth rate parameter a obtained from stochastic simulations (blue dots) compared with formula (28) (blue solid line).

B. Expansion rate for the Moore neighborhood

Using the method of Fig. 8(a) adapted to the Moore neighborhood, we find numerically that $\beta_M \approx 1.27$. The density formula is given by the solution of system (A8)–(A12) in the SM [27], or, more concisely (with slightly larger error), by Eq. (4). Similarly, the average fraction of neighbors that are not in the circle's interior is given by $\nu_M \approx 0.70$. Figure 8(b) compares the results from stochastic simulations with formula (28), using β_M and ν_M for β and ν.

In Fig. 8(b) we also see that expansion happens faster under the Moore neighborhood. This can be intuitively understood by noting that, with a larger number of points that count as neighbors, an individual has more choices for placing its offspring. In the case of a mass action (not shown), expansion is fastest and exponential in time.

VI. DISCUSSION

In this paper we developed deterministic approximations for the expected trajectories of a two-dimensional stochastic birth-death process. In particular, we focused on modeling 2D growth expanding radially from an origin o, a problem known in the literature as range expansion. We began by considering approximations based on the decoupling ideas of the *pair approximation* (PA); we referred to these approximations as *spatially explicit decoupling approximations*, or SEDA. For each SEDA we defined an order: A SEDA of nth order preserves correlations between neighbors that are n or less units of distance apart from each other. We found that first-order SEDA approximates the results from the stochastic process better than the mean-field or PA models; and second order improves on the first-order approximation. However, none of these models exhibit good time series agreement with the stochastic process.

There are two important differences between PA and SEDA. (1) PA models are nonspatial. They track only the total number of individuals, not the spatial location of each individual. SEDA is fully spatial. (2) PA models only consider correlations of pairs, while depending on the order; SEDA models can preserve correlations for larger groups of neighbors (e.g., up to quintuplets in second-order equations).

Next, we developed what we called *radial decoupling approximations*, or RDA. Here, an approximation involving a triad of sites depends on the location of the triad's center relative to the population origin. A system based only on RDA does not have a unique steady state; RDA, however, will be very useful when combined with SEDA. This approach lead us to the *trigonometric decoupling approximations*, or TDA. The name comes from the use of trigonometric functions in the approximations. We find that the TDA provides very good agreement with the stochastic process. We then revisited first-order SEDA, and found that scaling time by a suitable parameter also produces very good agreement with stochastic results.

The methods described above allow us to approximate the steady-state density of populations (or the density in the core of expanding colonies). In particular, we provide three simple formulas that approximate the equilibrium density: for the von Neumann and Moore neighborhoods on a square lattice, and for a honeycomb neighborhood on a hexagonal lattice; see Eqs. (2), (3), and (4). For the same death-to-birth ratio, the grid is more packed under the Moore neighborhood, because of the availability of more neighbors per site. As a consequence, the equilibrium density corresponding to the Moore neighborhood is higher and closer to that of mass action. A general formula that provides an approximation for the steady-state density as a function of the number of neighbors is given by Eq. (5). It describes the three cases in 2D that were mentioned above, and can also be derived in 3D for the von Neumann and Moore neighborhoods. The validity of this formula for other cases remains to be checked.

Finally, we turned our attention to the expected growth rate of an expanding population in an infinite grid. By focusing on the dynamics at the population's surface (or boundary), we found a simple explicit formula, Eq. (27), that estimates the evolution of the total number of individuals as a function of time. The growth law in (27) is the so called "surface growth" law [31], previously described in modeling literature [32–36]. Equation (28) provides a method to approximate the rate of surface growth from the "microscopic" rules and rates that govern the spatial birth-death process. This method involves knowledge of a population steady-state density and the geometric properties of disk-like objects on a square lattice, both of which depend on neighborhood type.

The methodology developed in the article can be adapted to include three-dimensional growth and other grid metrics. In 3D there are four equations per site for all first-order approximations using the ℓ_1 metric. SEDA and TDA approximations can also be developed for Moore neighborhoods (based on the ℓ_∞ norm). Using Moore neighborhoods in 2D, for example, leads to ten equations per grid point for first-order SEDA. Another important extension of the methodology is the inclusion of populations with more than one species. For example, in 2D with the ℓ_1 metric, for a two-species birth-death process there are ten equations per point for first-order approximations: two for the expected value of singletons (one per species), four for correlations of pairs of the same species, and four more for correlations of mixed pairs. For more complex models, such as those involving two or more species, the process of generating equations can be automated using MATHEMATICA, by first working out a pattern and then implementing equation generation in a program, a methodology similar to that used in [37].

Applying the methodology to more than one species can lead to important biological applications. For example, in the context of tumor growth, a two-species birth-death model can be easily adapted to account for feedback interactions between tumor stem cells and differentiated cells [38]. Similar adaptations can be used to model viral infection and the

interplay between infected and uninfected cells [39]. Another fundamental application is studying mutant dynamics in a spatial setting, which is relevant to a host of phenomena ranging from 2D bacterial evolution in biofilms to 3D evolutionary dynamics of cancer. In particular, the ideas used to estimate the population's expected growth rate (for one specie), could be applied to approximate the expected number of mutants as a function of time. The extensions to the theory and approximations discussed here can form the basis of these and other applications, and will be the focus of future work.

ACKNOWLEDGMENTS

I.A.R.-B., D.W., and N.L.K. designed the research; I.A.R.-B. and N.L.K. performed the research; I.A.R.-B. and N.L.K. wrote the paper. This work was funded by NSF Grant No. DMS-1815406.

[1] Q. Wang and T. Zhang, Review of mathematical models for biofilms, Solid State Commun. **150**, 1009 (2010).
[2] K. A. Rejniak and A. R. A. Anderson, Hybrid models of tumor growth, Wiley Interdiscip. Rev.: Syst. Biol. Med. **3**, 115 (2011).
[3] J. Landry, J. P. Freyer, and R. M. Sutherland, A model for the growth of multicellular spheroids, Cell Proliferation **15**, 585 (1982).
[4] J. E. Barralet, L. Wang, M. Lawson, J. T. Triffitt, P. R. Cooper, and R. M. Shelton, Comparison of bone marrow cell growth on 2D and 3D alginate hydrogels, J. Mater. Sci.: Mater. Med. **16**, 515 (2005).
[5] A. L. Koch, The growth of viral plaques during the enlargement phase, J. Theor. Biol. **6**, 413 (1964).
[6] J. Fort and V. Méndez, Time-Delayed Spread of Viruses in Growing Plaques, Phys. Rev. Lett. **89**, 178101 (2002).
[7] S. T. Abedon and J. Yin, Bacteriophage plaques: Theory and analysis, in *Bacteriophages* (Springer, Berlin, 2009), pp. 161–174.
[8] S. Fedotov, D. Moss, and D. Campos, Stochastic model for population migration and the growth of human settlements during the neolithic transition, Phys. Rev. E **78**, 026107 (2008).
[9] H. Taubenböck, M. Wurm, C. Geiß, S. Dech, and S. Siedentop, Urbanization between compactness and dispersion: Designing a spatial model for measuring 2D binary settlement landscape configurations, Int. J. Digital Earth **12**, 679 (2019).
[10] J. Moreira and A. Deutsch, Cellular automaton models of tumor development: A critical review, Adv. Complex Syst. **5**, 247 (2002).
[11] I. Santé, A. M García, D. Miranda, and R. Crecente, Cellular automata models for the simulation of real-world urban processes: A review and analysis, Landscape Urban Plann. **96**, 108 (2010).
[12] G. An, Q. Mi, J. Dutta-Moscato, and Y. Vodovotz, Agent-based models in translational systems biology, Wiley Interdiscip. Rev.: Syst. Biol. Med. **1**, 159 (2009).
[13] H. Byrne and D. Drasdo, Individual-based and continuum models of growing cell populations: A comparison, J. Math. Biol. **58**, 657 (2009).
[14] Z. Wang, J. D. Butner, R. Kerketta, V. Cristini, and T. S. Deisboeck, Simulating cancer growth with multiscale agent-based modeling, Semin. Cancer Biol. **30**, 70 (2015).
[15] N. G. Van Kampen, *Stochastic Processes in Physics and Chemistry*, Vol. 1, 3rd ed. (Elsevier, Amsterdam, 2007).
[16] V. Volpert and S. Petrovskii, Reaction–diffusion waves in biology, Phys. Life Rev. **6**, 267 (2009).
[17] S. P. Ellner, A. Sasaki, Y. Haraguchi, and H. Matsuda, Speed of invasion in lattice population models: Pair-edge approximation, J. Math. Biol. **36**, 469 (1998).
[18] S. P. Ellner, Pair approximation for lattice models with multiple interaction scales, J. Theor. Biol. **210**, 435 (2001).
[19] J. Joo and J. L. Lebowitz, Pair approximation of the stochastic susceptible-infected-recovered-susceptible epidemic model on the hypercubic lattice, Phys. Rev. E **70**, 036114 (2004).
[20] C. T. Bauch, The spread of infectious diseases in spatially structured populations: An invasory pair approximation, Math. Biosci. **198**, 217 (2005).
[21] J. Benoit, A. Nunes, and M. Telo da Gama, Pair approximation models for disease spread, Eur. Phys. J. B **50**, 177 (2006).
[22] E. Pugliese and C. Castellano, Heterogeneous pair approximation for voter models on networks, Europhys. Lett. **88**, 58004 (2009).
[23] X.-F. Luo, X. Zhang, G.-Q. Sun, and Z. Jin, Epidemical dynamics of SIS pair approximation models on regular and random networks, Physica A **410**, 144 (2014).
[24] A. S. Mata, R. S. Ferreira, and S. C. Ferreira, Heterogeneous pair-approximation for the contact process on complex networks, New J. Phys. **16**, 053006 (2014).
[25] H. Matsuda, N. Ogita, A. Sasaki, and K. Satō, Statistical mechanics of population: The Lattice Lotka-Volterra model, Prog. Theor. Phys. **88**, 1035 (1992).
[26] M. A. Gibson and J. Bruck, Efficient exact stochastic simulation of chemical systems with many species and many channels, J. Phys. Chem. A **104**, 1876 (2000).
[27] See Supplemental Material at http://link.aps.org/supplemental/10.1103/PhysRevE.101.032404 for derivations of higher order SEDA, steady-state under Moore neighborhoods, polynomial regressions for auxiliary parameters, and Supplementary Figures.
[28] E. A. van Doorn and P. K. Pollett, Quasi-stationary distributions for discrete-state models, Eur. J. Oper. Res. **230**, 1 (2013).
[29] I. A. Rodriguez-Brenes, D. Wodarz, and N. L. Komarova, Quantifying replicative senescence as a tumor suppressor pathway and a target for cancer therapy, Sci. Rep. **5**, 17660 (2015).
[30] A. Hofacre, D. Wodarz, N. L. Komarova, and H. Fan, Early infection and spread of a conditionally replicating adenovirus under conditions of plaque formation, Virology **423**, 89 (2012).
[31] M. Block, E. Schöll, and D. Drasdo, Classifying the Expansion Kinetics and Critical Surface Dynamics of Growing Cell Populations, Phys. Rev. Lett. **99**, 248101 (2007).
[32] A. Brú, S. Albertos, J. L. Subiza, J. L. García-Asenjo, and I. Brú, The universal dynamics of tumor growth, Biophys. J. **85**, 2948 (2003).
[33] N. L. Komarova and D. Wodarz, Ode models for oncolytic virus dynamics, J. Theor. Biol. **263**, 530 (2010).

[34] I. A. Rodriguez-Brenes, N. L. Komarova, and D. Wodarz, Tumor growth dynamics: Insights into evolutionary processes, Trends Ecol. Evol. **28**, 597 (2013).

[35] A. Talkington and R. Durrett, Estimating tumor growth rates in vivo, Bull. Math. Biol. **77**, 1934 (2015).

[36] H. Murphy, H. Jaafari, and H. M. Dobrovolny, Differences in predictions of ode models of tumor growth: A cautionary example, BMC Cancer **16**, 163 (2016).

[37] A. Mahdipour-Shirayeh, A. H. Darooneh, A. D. Long, N. L. Komarova, and M. Kohandel, Genotype by random environmental interactions gives an advantage to non-favored minor alleles, Sci. Rep. **7**, 5193 (2017).

[38] I. A. Rodriguez-Brenes, N. L Komarova, and D. Wodarz, Evolutionary dynamics of feedback escape and the development of stem-cell-driven cancers, Proc. Natl. Acad. Sci. USA **108**, 18983 (2011).

[39] I. A. Rodriguez-Brenes, A. Hofacre, H. Fan, and D. Wodarz, Complex dynamics of virus spread from low infection multiplicities: Implications for the spread of oncolytic viruses, PLoS Comput. Biol. **13**, e1005241 (2017).